

Converged Velocity Field for Rotors by a Blended Potential Flow Method

Jianzhe Huang, David A. Peters, J.V. R. Prasad

Abstract— Potential-flow solutions for rotor induced flow by the He method give good convergence on the disk but can provide only a crude approximation off of the disk. The Morillo-Duffy formulation can give all three components off the disk, but the results converge poorly on the disk. Furthermore, Morillo-Duffy solutions converge very slowly for the velocity downstream in the limit as wake skew angle approaches 90° (edgewise flow). In this work, new variables—called the Nowak-He variables—are introduced that provide both the He velocity and the Morillo-Duffy velocity from a single set of states. In addition, an approximate downstream velocity field is obtained from the adjoint theorem that gives the exact downstream velocity as skew angle approaches 90°. The blending of these three velocity fields is shown to give robust and accurate convergence to the potential-flow equations at all flight conditions.

Keywords—potential flow; downstream velocity; Nowak-He solution; Morillo-Duffy solution

LIST OF SYMBOLS

$[A]$:	transform matrix	V_{NC} :	normal induced velocity based on Nowak-He variable
a_j^m :	Morillo-Duffy variables	V_F :	final induced velocity
α_n^m :	Nowak-He variables	V_{DS} :	downstream limiting velocity
m :	harmonic numbers	χ :	skew angle
n, j :	polynomial numbers	τ_1^0 :	elliptical pressure coefficient
$P_n^m(v)$:	normalized Legendre function of first kind	σ :	distance along x-axis from $(-s_0)$ to the point at which the velocity is desired, $\sigma = (-x - s_0)$
$Q_n^m(i\eta)$:	normalized Legendre function of second kind	x, y, z :	non-dimensional rotor disk coordinates, coordinate divided by R
R :	rotor radius, m	v, η, ψ :	ellipsoidal coordinates
ζ :	non-dimensional coordinate along free-stream line, positive below disk	v_0, η_0, ψ_0 :	the ellipsoidal coordinates of the intersection point of rotor plane and the free-stream line
s :	distance from the point of velocity computation along a streamline to the rotor disk at r_0, ψ_0	ω :	reduced frequency, $\omega = \Omega R / V_\infty$
s_0 :	x-distance downstream in edgewise flow, m	Ω :	rotor speed, rad/sec
t :	time, sec	$m!!$:	double factorial, $m(m-2)(m-4)\dots$
V_∞ :	free-stream velocity, m/sec	x_0 :	non-dimensional location of streamline intersection with disk, distance/ R
V_{MD} :	normal induced velocity based on Morillo-Duffy variable		

I. BACKGROUND

The incompressible potential-flow equations serve well to predict the rotor wake during powered flight. Traditional vortex-lattice and vortex-panel methods do an excellent job of solving these equations, but they are often too inefficient for real-time flight simulation. Therefore, a class of finite-state inflow models has been developed based on application of the Galerkin method in order to obtain a set of low-order, state-variable equations. Peters and He [1] developed a potential-flow theory for the vertical component of flow at the rotor disk. They validated the model against wind-tunnel data, as in [2, 3]. The Peters-He model is widely used in many production codes including FLIGHTLAB (Advanced Rotorcraft Technology), COPTER (Bell Helicopter), RCAS (U. S. Government) and ONERA-DFVLR (European Community), etc.

In 1996, Wen-Ming Cao [4] made an attempt to compute the flow off of the rotor disk by a similar model. His work demonstrated that there must be a

second set of wake states for flow off the rotor to be calculated, but he was unable to determine them. Morillo showed that these states could be found rigorously, as in [5, 6]. Morillo wrote a generalized velocity potential and expanded that potential in terms of Legendre functions. By including both odd and even functions—and treating them as velocity potentials—Morillo was able to use a Galerkin approach to obtain a closed-form set of equations for all components of velocity above and on the plane of the rotor disk. All matrices are in closed form, and mass sources are also allowed.

The Morillo model gives excellent agreement with closed-form solutions for step response and frequency response, but convergence is slow due to ill-conditioned matrices. In 2005, Michael Ke Yu [7] demonstrated that the ill-conditioning was due to a lack of certain singular expansion functions. Hsieh [8] derived closed-form expressions for these singular functions; and Garcia-Duffy [9] incorporated them into a complete dynamic inflow model for all components of flow in the upper hemisphere. A summary of this inflow development can be found in [10].

Recently, Fei [11, 12] extended Morillo’s model and found a rigorous solution for the flow below the plane of the rotor, which allows application of finite-state methods within the rotor wake—giving the entire velocity field at all points. The ability to find the flow field everywhere impacts not only rotor flight simulation but also wind energy applications, as in [13]. It is also interesting to note that the three-dimensional inflow model has an analog in two-dimensional flow and can be applied to airfoil theory, as in [14]. This has also led to applications to the locomotion of organisms by the above finite-state methodology, as in [15]. The cost of this transaction is that one must also compute the adjoint of the velocity (i.e., the co-states of the flow). Once that is done, the complete flow below the plane follows directly. The co-state method insures that the flow below the disk converges at least as well as the flow above the disk. The adjoint methodology has been validated for both step response and frequency response throughout the range of skew angles.

The major drawbacks of the Finite-State inflow of Fei have been: 1.) It is not as well-conditioned as the He model for inflow on the disk; and 2.) It diverges downstream as the skew angle approaches 90° (edgewise flow). The reason for the first drawback is that the inflow model of He was derived in two separate forms. One form uses the natural Legendre functions $P_n^m(\nu)$ for the velocity expansion. The second form uses a transform to write the velocities in terms of the functions $P_n^m(\nu)/\nu$ which are polynomials in r . Because the second version (with the polynomials) converges much faster than the first, subsequent applications have used this second form. However, because the second form uses functions that are not the natural Laplacean solutions, the Fei model

could not utilize them. It rather uses the poorly-converging $P_n^m(\nu)$.

In this paper, we show that one can compute both the He second-form variables (which we call the Nowak-He variables) and the Morillo-Duffy variables from a single set of unified inflow states. The Nowak-He and Morillo-Duffy solutions are computed through a change of variable. Those solutions can then be blended to obtain the well-behaved He solution on the disk and the accurate Morillo-Duffy solution away from the disk. The blending is taken such that one need not calculate Morillo-Duffy velocity either on the disk or close to the disk edge, where it is ill-conditioned, Nowak [16].

For the second deficiency, the major issue is that, as the flow becomes edgewise, the trailing wake moves closer and closer to the downstream rotor plane—so that the induced flow downstream does not decay. As a result, the Legendre Functions (which all decay) are unable to converge to the velocity downstream. To remove this deficiency, the adjoint theorem has been extended to the case of perfectly edgewise flow to show that the flow downstream can be computed from the velocity and adjoint velocity upstream.

To compute the downstream velocity from the adjoint velocity requires the computation of no additional states—only the use of existing information. That solution can then be blended with the previously-blended Nowak-He and Morillo-Duffy variables. The blending is defined such that, for perfectly-edgewise flow, we use only the limiting downstream velocity (which is exact); and, for axial flow, we use only the true blended Nowak-He/Morillo-Duffy solution, which has no convergence problems away from edgewise flow. Finally, the flow below the disk is found in the normal way from the completely blended velocity and adjoint velocity above the disk. This paper is based on work presented earlier in [17].

II. EXTENDED BLENDING METHOD

For the extended blending method, the He (which is also called Nowak-He) and the Morillo-Duffy solution are combined. The Morillo-Duffy variables are transformed from Nowak variables via the transform matrix $[A]$. The equation is expressed as

$$\{a_j^m\} = [A_{nj}^m]^{-1} \{\alpha_n^m\} \quad (1)$$

$$[A_{nj}^m] = \frac{(-1)^{\frac{n+j-2r}{2}} 2\sqrt{2n+1}\sqrt{2j+1}}{\sqrt{H_n^r} \sqrt{H_j^r} (n+j)(n+j+2) [(n-j)^2 - 1]} \quad (2)$$

$$H_n^m = \frac{(n+m-1)!(n-m-1)!!}{(n+m)!!(n-m)!!} \quad (3)$$

where $\{a_j^m\}$ and $\{\alpha_n^m\}$ are Morillo-Duffy variables and Nowak-He variable, respectively.

Then the normal induced velocity above the rotor disk ($z < 0$) based on Morillo-Duffy variable and Nowak-He variables can be obtained by

$$V_{MD} = \sum_{m,n}^{\infty} \alpha_n^m P_n^m(v) Q_n^m(i\eta) \cos(m\psi) \quad (4)$$

$$V_{NH} = \sum_{\substack{m,n \\ odd}}^{\infty} \alpha_n^m \frac{1}{v} P_n^m(v) Q_{m+1}^m(i\eta) \cos(m\psi) \\ + \sum_{\substack{m,n \\ even}}^{\infty} \alpha_n^m P_n^m(v) Q_{m+1}^m(i\eta) \cos(m\psi) \quad (5)$$

The adjoint velocity based on Morillo-Duffy method and Nowak-He is given as follows as well.

$$V_{MD}^* = \sum_{m,n}^{\infty} \Delta_n^m P_n^m(v) Q_n^m(i\eta) \cos(m\psi) \quad (6)$$

$$V_{NH}^* = \sum_{\substack{m,n \\ odd}}^{\infty} \Delta_n^m \frac{1}{v} P_n^m(v) Q_{m+1}^m(i\eta) \cos(m\psi) \\ + \sum_{\substack{m,n \\ even}}^{\infty} \Delta_n^m P_n^m(v) Q_{m+1}^m(i\eta) \cos(m\psi) \quad (7)$$

where $\{\Delta_n^m\}$ and $\{\Lambda_n^m\}$ are Morillo-Duffy adjoint variables and Nowak-He adjoint variables, respectively. For the special case ($\omega = 0$), we have

$$\{\Delta_n^m\} = \{\alpha_j^m\} \text{ and } \{\Lambda_n^m\} = \{\alpha_n^m\} \quad (8)$$

Since the Nowak-He solution behaves well on the the disk and the Morillo-Duffy solution is more accurate away from the disk, the blending function which is given in (9-10) is designed to transition quickly to Morillo-Duffy.

$$V_{BL} = \frac{1}{1+bh} V_{NH} + \frac{bh}{1+bh} V_{MD} \quad (9)$$

$$V_{BL}^* = \frac{1}{1+bh} V_{NH}^* + \frac{bh}{1+bh} V_{MD}^* \quad (10)$$

where

$$\begin{cases} h = 0, & \text{if } \eta < \varepsilon \\ h = \eta - \varepsilon, & \text{if } \eta \geq \varepsilon \end{cases} \quad (11)$$

and where

$$\begin{aligned} x \leq 0, |y| \leq 1, b = 20 & \left[1 - \frac{y^2 \sin(\chi)}{1 + \eta^2} \right] \\ x \leq 0, |y| > 1, b = 20 & \left[1 - \frac{y^2 \sin(\chi)}{1 + \eta^2 + 0.615(y^2 - 1)} \right] \\ x > 0, |y| \leq 1, b = 20 & \left[1 - \frac{(x^2 + y^2) \sin(\chi)}{1 + \eta^2} \right] \\ x > 0, |y| > 1, b = 20 & \left[1 - \frac{(x^2 + y^2) \sin(\chi)}{1 + \eta^2 + 0.615(y^2 - 1)} \right] \end{aligned} \quad (12)$$

One need not to calculate Morillo-Duffy velocity either on the disk or close to the disk edge ($\varepsilon = 0.01$) where it is ill-conditioned.

As the flow becomes edgewise, the induced flow downstream does not decay due to the trailing wake effect. Therefore, the adjoint theorem has been extended to the case of perfectly edgewise flow.

Let s_0 be the x-distance downstream in edgewise flow at which the flow is converged by the blended method. We take this distance to be on a sphere of radius one or else to be zero if $y^2 + z^2 \geq 1$.

$$\begin{cases} s_0 = \sqrt{1 - y^2 - z^2}, & \text{for } y^2 + z^2 < 1 \\ s_0 = 0, & \text{for } y^2 + z^2 \geq 1 \end{cases} \quad (13)$$

Let x be a point (further downstream than $-s_0$) at which the velocity is desired. Let the distance along the x -axis from ($-s_0$) to that point at which the velocity is desired be called $\sigma = (-x - s_0)$. It follows that the distance along the streamline going through $-s_0$ to the point on the streamline that is closest to x (i.e., perpendicular) is then given by $\sigma \sin(\chi)$. We then define the time delay for adjoint theorem to be $\sigma \sin(\chi)$.

Thus, in the plane of the disk, $z = 0$ and $1 < y < -1$, one should place s_0 at the trailing edge of the disk (region ①); $s_0 = 0$ for $z = 0$ and $|y| > 1$ (region ②) which is illustrated in Fig. 1. The thick solid curve denotes the trailing edge of the rotor disk.

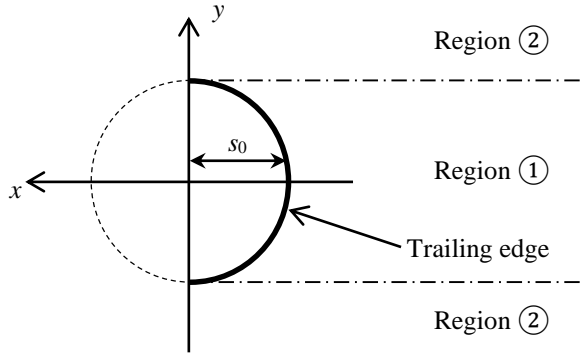


Figure Illustration of downstream in edgewise flow at the rotor disk.

Then the downstream velocity ($x \leq 0$ and $|x^2 + y^2 + z^2| \geq 0$) can be found from the adjoint theorem:

$$\begin{aligned} V_{DS}(x, y, z, t) &= V_{DS}(-\sigma - s_0, y, z, t) \\ &= V_{BL}(-s_0, y, z, t - \sigma \sin(\chi)) \\ &\quad + V_{BL}^*(+s_0, -y, z, t - \sigma \sin(\chi)) \\ &\quad - V_{BL}^*(\sigma + s_0, -y, z, t) \end{aligned} \quad (14)$$

$$\begin{aligned} V_{DS}^*(x, y, z, t) &= V_{DS}^*(-\sigma - s_0, y, z, t) \\ &= V_{BL}^*(-s_0, y, z, t + \sigma \sin(\chi)) \\ &\quad + V_{BL}(+s_0, -y, z, t + \sigma \sin(\chi)) \\ &\quad - V_{BL}(\sigma + s_0, -y, z, t) \end{aligned} \quad (15)$$

Based on (9) and (14), one can obtain the downstream final velocity V_F from V_{BL} and V_{DS} which is shown in (16). For both on the disk and upstream ($x > -s_0$), $V_F = V_{BL}$. Similarly, the adjoint V_F^* is given in (17) through a combination of (10) and (15).

$$V_F = V_{BL}[1 - f(s_0, \eta)] + V_{DS}[f(s_0, \eta)] \quad (16)$$

$$V_F^* = V_{BL}^*[1 - f(s_0, \eta)] + V_{DS}^*[f(s_0, \eta)] \quad (17)$$

where

$$f(\sigma, \chi) = \begin{cases} \frac{\sin^2(\chi)}{\sin^2(\chi) + \sigma g(\chi)}, & \text{for } |y| \leq 1 \\ \frac{\sin^2(\chi)}{\sin^2(\chi) + (\sigma + 1.5\sqrt{y^2 - 1})g(\chi)}, & \text{for } |y| > 1 \end{cases} \quad (18)$$

where

$$g(\chi) = 1.84 \cos^{1/2}(\chi) - 4.06 \cos(\chi) + 11.84 \cos^{3/2}(\chi) \quad (19)$$

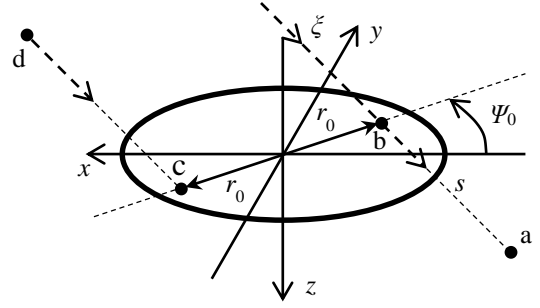


Figure 2 3-D perspective of co-states

Fig. 2 shows the 3-D perspective of the co-state method. For the velocity at point a (below the disk), one should compute the velocity at point b , which is the intersection point of the free streamline and the rotor plane first, then add the adjoint velocity at point c , which is centrosymmetric to point b in the disk plane, minus the adjoint velocity at point d , which is centrosymmetric to point a above the rotor disk. s is the distance from point a along the streamline to the rotor disk (point b) at r_0 , ψ_0 .

$$\begin{aligned} V(t, x, y, z) &= V(t, z, r, \psi) \\ &= V_F(t - s, 0, r_0, \psi_0) \\ &\quad + V_F^*(t - s, 0, r_0, \psi_0 + \pi) \\ &\quad - V_F^*(t, -z, r, \psi + \pi) \end{aligned} \quad (20)$$

The above derivation is for the z component of velocity, which is perpendicular to the rotor disk. For the x and y components, there is no counterpart in the Nowak-He model. Thus, the blended velocities of (9-10) are replaced by V_{MD} for both the x and y components: $V_{BL} \equiv V_{MD}$, $V_{BL}^* \equiv V_{MD}^*$. It follows that V_{DS} is then formed the same way for V_x and V_y as it is for V_z in (14-15). However, because the x and y derivatives of the velocity potential have the opposite even-function and odd-function behavior as does the z derivative (upwind and downwind), the signs of the adjoint velocities in (14-15) are opposite for V_x and V_y from those in (14-15) for V_z downstream. The blending for V_x and V_y according to (16-19) then follows with the exception that $f(s_0, \eta)$ should be multiplied by $[1 - \cos(\chi)]^{5/3}$ for V_x and V_y . For velocity below the disk, there is no difference in the blending algorithm for x and y components as compared to z component. In this paper, we only consider V_z .

III. RESULTS

With the blending method discussed above, some typical results (four skew angles, two frequencies, and various cuts through the flow field) are presented to

show the degree of accuracy of the solution. Results are for the z -component (normal component) of velocity. Some results have 6 harmonic for the odd terms and 4 harmonics for the even terms (25 states). Other results have 12 harmonics for the odd terms and 8 harmonics for even terms (74 states). For example:

m-odd = 12, m-even = 8 for $\omega = 0$

m-odd = 12, m-even = 8 for $\omega = 4$ and $0^\circ < \chi \leq 45^\circ$

m-odd = 6, m-even = 4 for $\omega = 4$ and $45^\circ < \chi \leq 90^\circ$

The rotor is given an elliptical pressure distribution. The axial coordinate is z , with $z > 0$ downstream. The fore-aft coordinate is x , with $x < 0$ being downstream. The lateral coordinate is y . The results for $\omega = 0$ (constant loading) and $\omega = 4$ (frequency = $4V_\infty / R$) are illustrated in Figs. 3-22. The open circles on the plots are the exact solution for each case, which can be found from a convolution integral from upstream infinity along a streamline down to that particular point. The solid lines are the new, blended solutions. For comparison, each figure shows the various velocities that are blended together to obtain the final solution. The dashed-dot blue line is the Morillo-Duffy solution. The long-dash green curve is the velocity from the Nowak-He variables.

Figs. 3-6 give induced velocity at the rotor disk ($y = 0.0$ and $z = 0.0$), for $\omega = 0$, and there are no imaginary parts in the solution. The skew angle is varied from 0° to 85° . Figs. 7 and 8 show the results for two cuts along the y axis ($y = 0.5$ and 1.26). Since the flow is symmetric about the y axis, only the induced velocity for $y \geq 0$ needs to be computed. Fig. 9 presents a y -traverse. Results above the disk ($z = -0.4$) are directly above the disk and are plotted versus x in Fig. 10. In Fig. 11, results below the disk ($z = +0.4$) are plotted from the center of the skewed wake versus x_0 , which is the x location on the rotor disk through which a streamline would pass. Thus, $x_0 = 0$ is the streamline going through the rotor center.

Fig. 3, which shows flow on the disk, shows axial flow so that the Morillo and He variables work equally well on the disk, and the “downstream” correction has no physical meaning (and is not blended). As skew angle is increased (Figs. 4-6), one can see the increase of downstream flow. The Nowak change of variable becomes more and more accurate (with respect to Duffy-Morillo) as skew angle increases, and the velocity begins to approach the “downstream” solution (which becomes the exact solution as skew angle approaches 90°). Notice that the blending function does an excellent job of combining the three solutions together to match the exact solution (from a convolution integral).

Fig. 8 is an x -plot located at 0.26 radii laterally from the edge of the disk. Although this is very close to the trailing vortex that comes off of the disk edge, the velocity is still quite good. Fig. 9 sheds further insight on this correlation by giving a plot of velocity versus lateral coordinate y off the edge of the disk.

The point $y=1.26$ marks the location of the cross-plot in Fig. 8. One can see that the peak due to the trailing vortex is well-captured with the appropriate decay off of the disk.

Figs. 10-11 give velocity 0.4 radii above the disk and 0.4 radii below the disk, respectively. The same good convergence at the disk is seen above the disk. Here, the He variables have less effect; and it is basically a blending of downstream and Morgan variables. Below the disk, the improvement of the downstream blending at the disk is magnified. This is because the flow below the disk (in the adjoint method) is sensitive to the flow at the disk. Fig. 12, which is a traverse above the disk, illustrates that this above disk correlation is good not simply at $z = -0.4$ but continues at all locations.

Ten similar cases for $\omega = 4$ are demonstrated in Figs. 13-22. The real part and imaginary part of the induced velocity are given in the separate plots. The results obtained through the blended method match the exact solution perfectly both upstream and downstream, above the rotor disk and below the disk.

The same trends as were seen for $\omega = 0$ in Figs. 3-12 are repeated at $\omega = 4$ in Figs. 13-22. In this second set of figures, there are both real and imaginary plots (for the in-phase and out-of-phase velocities); but the same trends persist as were found for the steady case. Figs. 16, 17, and 21 clearly show the oscillations in the induced flow behind the disk. This is due to the fact that vorticity is being shed into the wake at a frequency of 4.0. Thus, there are oscillations in the velocity downstream that decay slowly (and which cease to decay at all as the skew angle approaches 90°). Notice that neither the Duffy-Morillo variables nor the Nowak-He variables can predict such oscillations, but the adjoint velocity gives the precise oscillations that are needed. After blending, the solution is virtually exact at all skew angles. This accuracy naturally persists downstream from the rotor disk, Fig. 21.

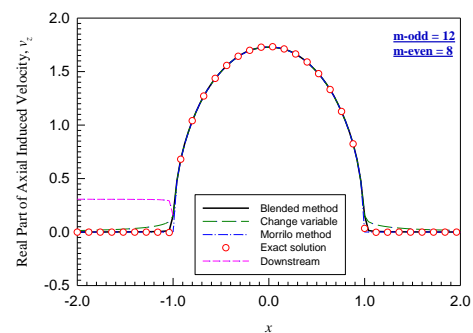


Figure 3 Real part of axial velocity V_z for $y = 0.0$, $z = 0.0$ with τ_1^0 for $\omega = 0$, $\chi = 0^\circ$. (m-odd = 12, m-even = 8)

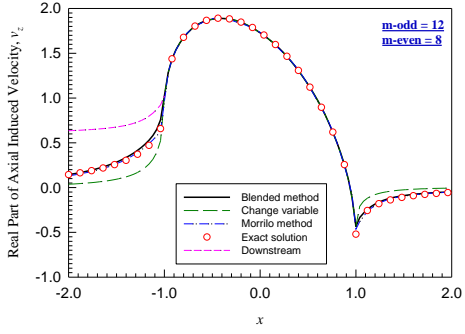


Figure 4 Real part of axial velocity V_z for $y = 0.0, z = 0.0$ with τ_1^0 for $\omega = 0, \chi = 30^\circ$. (m-odd = 12, m-even = 8)

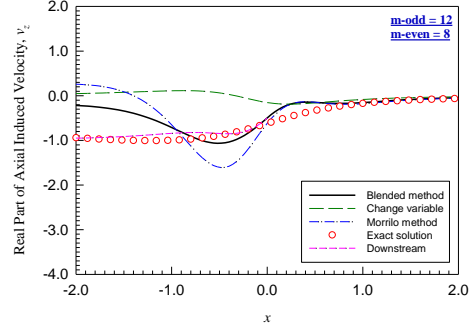


Figure 8 Real part of axial velocity V_z for $y = 1.26, z = 0.0$ with τ_1^0 for $\omega = 0, \chi = 85^\circ$. (m-odd = 12, m-even = 8)

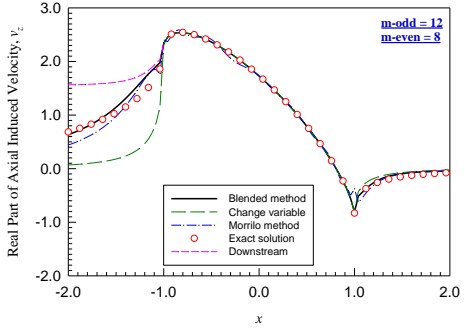


Figure 5 Real part of axial velocity V_z for $y = 0.0, z = 0.0$ with τ_1^0 for $\omega = 0, \chi = 60^\circ$. (m-odd = 12, m-even = 8)

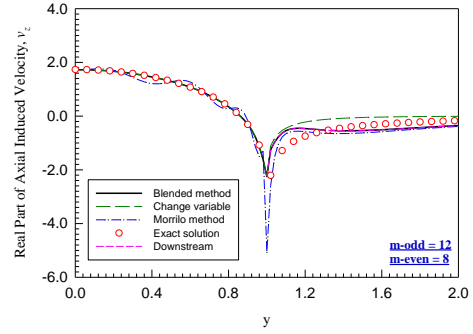


Figure 9 Real part of axial velocity V_z for $x = 0.0, z = 0.0$ with τ_1^0 for $\omega = 0, \chi = 85^\circ$. (m-odd = 12, m-even = 8)

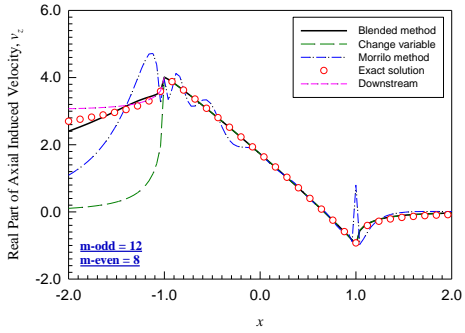


Figure 6 Real part of axial velocity V_z for $y = 0.0, z = 0.0$ with τ_1^0 for $\omega = 0, \chi = 85^\circ$. (m-odd = 12, m-even = 8)

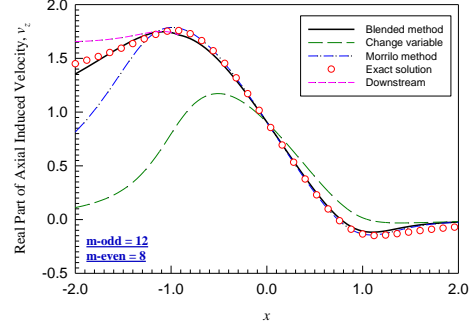


Figure 10 Real part of axial velocity V_z for $y = 0.0, z = -0.4$ with τ_1^0 for $\omega = 0, \chi = 85^\circ$. (m-odd = 12, m-even = 8)

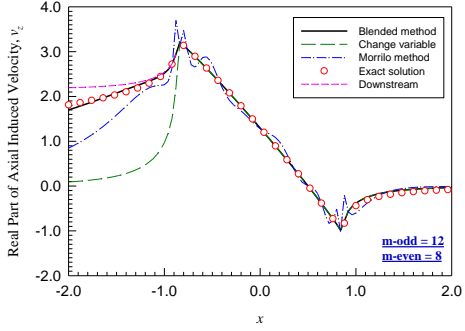


Figure 7 Real part of axial velocity V_z for $y = 0.5, z = 0.0$ with τ_1^0 for $\omega = 0, \chi = 85^\circ$. (m-odd = 12, m-even = 8)

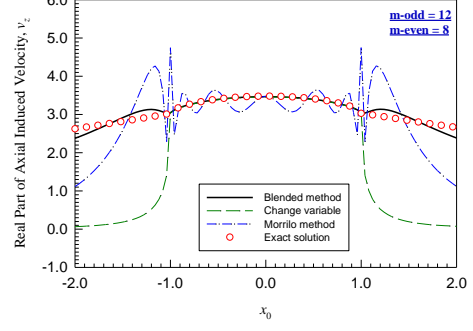


Figure 11 Real part of axial velocity V_z for $y = 0.0, z = 0.4$ with τ_1^0 for $\omega = 0, \chi = 85^\circ$. (m-odd = 12, m-even = 8)

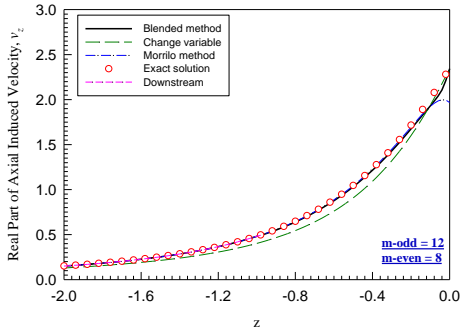
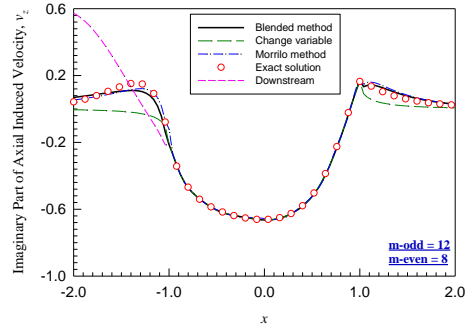
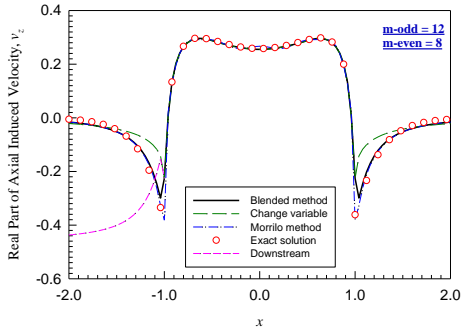


Figure 12 Real part of axial velocity V_z for $x = -0.25, y = 0.0$ with τ_1^0 for $\omega = 0, \chi = 85^\circ$. (m-odd = 12, m-even = 8)

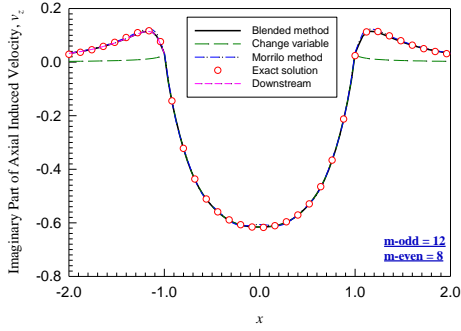


(b)

Figure 14 Axial velocity V_z for $y = 0.0, z = 0.0$ with τ_1^0 for $\omega = 4, \chi = 30^\circ$: (a) real part and (b) imaginary part. (m-odd = 12, m-even = 8)

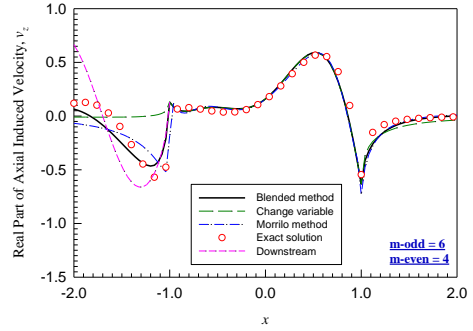


(a)

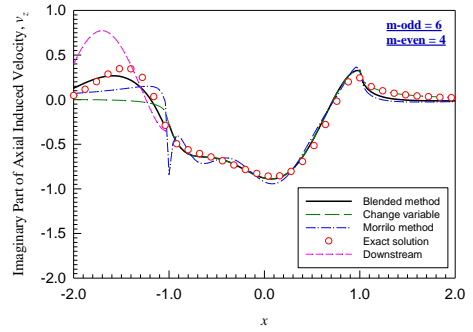


(b)

Figure 13 Axial velocity V_z for $y = 0.0, z = 0.0$ with τ_1^0 for $\omega = 4, \chi = 0^\circ$: (a) real part and (b) imaginary part. (m-odd = 12, m-even = 8)

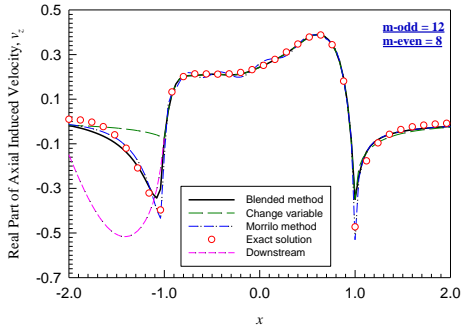


(a)

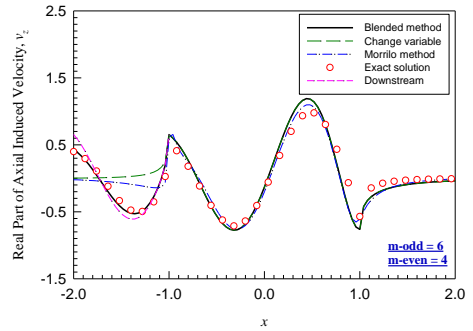


(b)

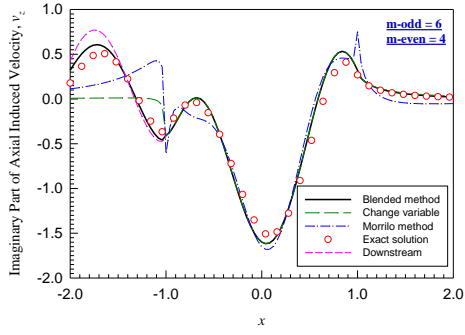
Figure 15 Axial velocity V_z for $y = 0.0, z = 0.0$ with τ_1^0 for $\omega = 4, \chi = 60^\circ$: (a) real part and (b) imaginary part. (m-odd = 6, m-even = 4)



(a)

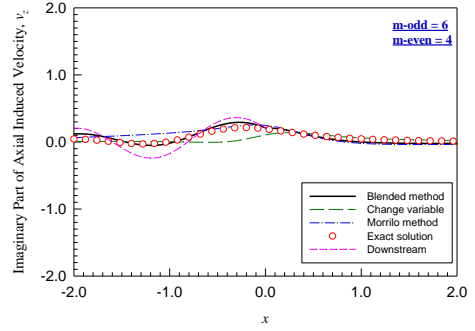


(a)



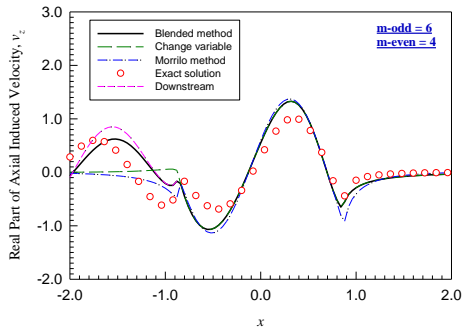
(b)

Figure 16 Axial velocity V_z for $y = 0.0, z = 0.0$ with τ_1^0 for $\omega = 4, \chi = 85^\circ$: (a) real part and (b) imaginary part. (m-odd = 6, m-even = 4)

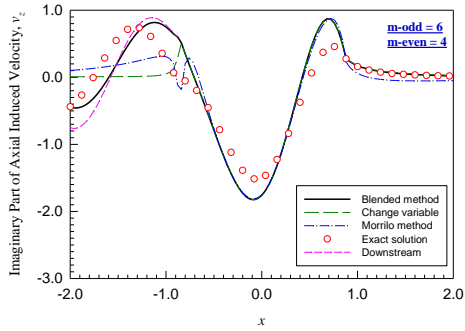


(b)

Figure 18 Axial velocity V_z for $y = 1.26, z = 0.0$ with τ_1^0 for $\omega = 4, \chi = 85^\circ$: (a) real part and (b) imaginary part. (m-odd = 6, m-even = 4)

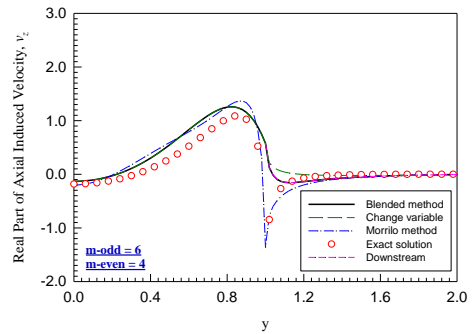


(a)

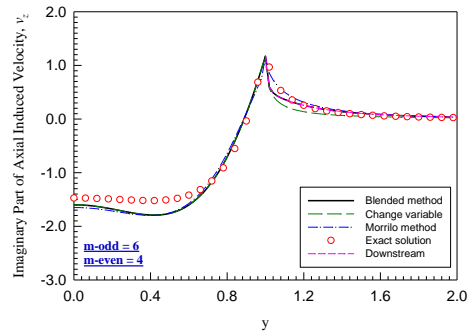


(b)

Figure 17 Axial velocity V_z for $y = 0.5, z = 0.0$ with τ_1^0 for $\omega = 4, \chi = 85^\circ$: (a) real part and (b) imaginary part. (m-odd = 6, m-even = 4)

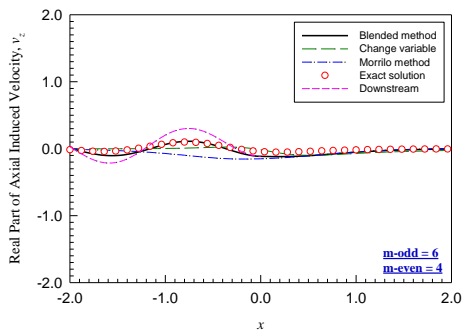


(a)

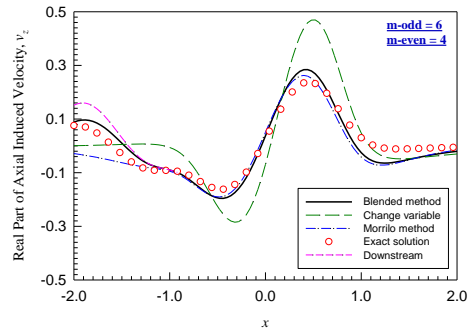


(b)

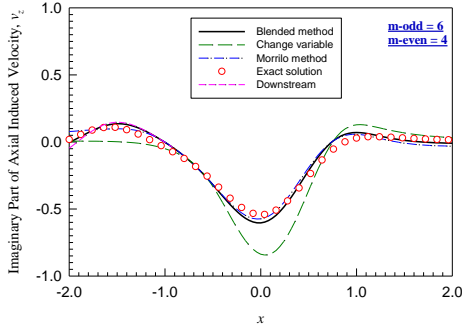
Figure 19 Axial velocity V_z for $x = 0.0, z = 0.0$ with τ_1^0 for $\omega = 4, \chi = 85^\circ$: (a) real part and (b) imaginary part. (m-odd = 6, m-even = 4)



(a)

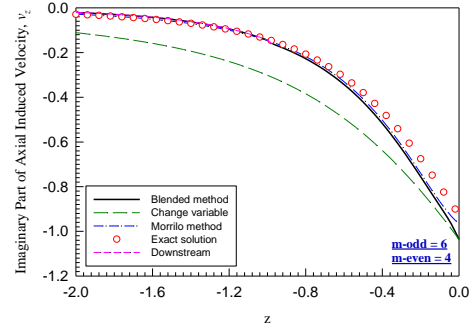


(a)



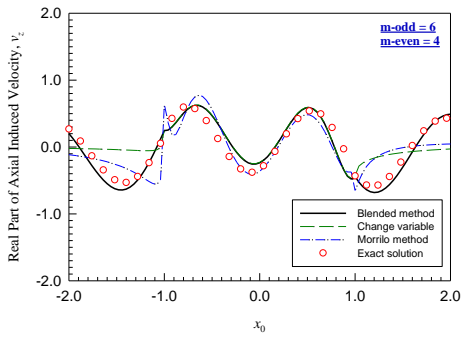
(b)

Figure 20 Axial velocity V_z for $y = 0.0$, $z = -0.4$ with τ_1^0 for $\omega = 4$, $\chi = 85^\circ$: (a) real part and (b) imaginary part. (m-odd = 6, m-even = 4)

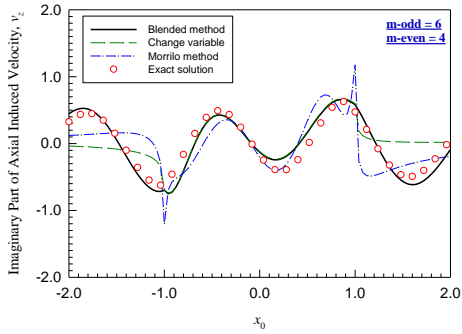


(b)

Figure 22 Axial velocity V_z for $x = -0.25$, $y = 0.0$ with τ_1^0 for $\omega = 4$, $\chi = 85^\circ$: (a) real part and (b) imaginary part. (m-odd = 6, m-even = 4)

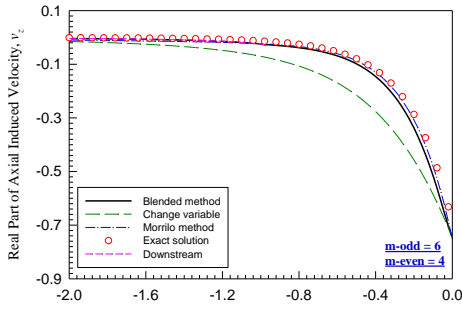


(a)



(b)

Figure 21 Axial velocity V_z for $y = 0.0$, $z = 0.4$ with τ_1^0 for $\omega = 4$, $\chi = 85^\circ$: (a) real part and (b) imaginary part. (m-odd = 6, m-even = 4)



(a)

IV. CONCLUSIONS

A new methodology is introduced to obtain rotor induced velocity either on the rotor disk or off the disk. To obtain good convergence at all skew angles, the Morillo-Duffy and Nowak-He velocity fields are blended with a closed-form downstream velocity (which is exact for perfectly edge-wise flow). The induced velocity below the rotor disk can also be obtained via this extended blending method. No new flow states are required for this method. Only normal and adjoint states are utilized. Comparisons with the exact solution for steady and unsteady flow verify the effectiveness of the new approach.

ACKNOWLEDGMENT

This work was sponsored by the Rotorcraft Centers of Excellence through the Georgia Tech/Washington University Center of Excellence, Drs. Michael Rutkowski and Robert Ormiston, technical monitors.

REFERENCES

- [1] Peters, David A., Boyd, David Doug, and He, Cheng Jian, "A Finite-State Induced-Flow Model for Rotors in Hover and Forward Flight," *Journal of the American Helicopter Society*, Vol. 34, No. 4, October 1989, pp. 5-17.
- [2] Peters, David A. and He, Cheng-Jian, "Correlation of Measured Induced Velocities with a Finite-State Wake Model," *Journal of the American Helicopter Society*, Vol. 36, No. 3, July 1991, pp. 59-70.
- [3] Su, Ay, Yoo, Kyung M., and Peters, David A., "Extension and Validation of an Unsteady Wake Model for Rotors," *Journal of Aircraft*, Vol. 29, No. 3, May-June 1992, pp. 374-383.
- [4] Peters, David A. and Cao, Wenming, "Off-Rotor Induced Flow by a Finite-State Wake Model," 37th AIAA SDM Conference, Salt Lake City, April 15-17, 1996, Paper No. 96-1550.
- [5] Morillo, Jorge and Peters, David A., "Velocity Field above a Rotor Disk by a New Dynamic Inflow Model," *Journal of Aircraft*, Vol. 39, No. 5, September-October 2002, pp. 731-738.
- [6] Peters, David A., Morillo, Jorge, and Nelson, Adria M., "New Developments in Dynamic Wake Modeling for

Dynamics Applications,” *Journal of the American Helicopter Society*, Vol. 48, No. 2, April 2003, pp. 120-127.

- [7] Yu, Ke and Peters, David A., “Nonlinear Three-Dimensional State-Space Modeling of Ground Effect with a Dynamic Flow Field,” *Journal of the American Helicopter Society*, Vol. 50, No. 3, July 2005, pp. 259-268.
- [8] Hsieh, Antonio, *A Complete Finite-State Model for Rotors in Axial Flow*, Master of Science Thesis, Washington University in St. Louis, August 2006.
- [9] Peters, David A., Hsieh, Antonio, and Garcia-Duffy, Cristina, “A Complete Finite-State Inflow Theory from the Potential Flow Equations,” 3rd International Basic Research Conference on Rotorcraft Technology, Nanjing, China, Oct. 14-16, 2009.
- [10] Peters, David A., “How Dynamic Inflow Survives in the Competitive World of Rotorcraft Aerodynamics,” the 2008 Alexander Nikolsky Lecture, *Journal of the American Helicopter Society*, Vol. 54, No. 1, January 2009, pp. 1-15.
- [11] Fei, Zhongyang and Peters, David A., “A Rigorous Solution for Finite-state Inflow throughout the Flowfield,” The 30th AIAA Applied Aero-dynamics conference, New Orleans, Louisiana, 2012.
- [12] Fei, Zhongyang and Peters, David A., “Inflow below the Rotor Disk for Skewed Flow by the Finite-State, Adjoint Method,” the 38th European Rotorcraft Forum, 2012
- [13] Peters, David A. and Modarres, Ramin, “A Compact Closed-Form Solution for the Optimum Induced-Flow Distribution of an Ideal Wind Turbine,” *Wind Energy*, 6 FEB. 2013| DOI: 10.1002/we.1597.
- [14] Peters, David A., “Two-Dimensional Incompressible Unsteady Airfoil Theory – An Overview,” *Journal of Fluids and Structures*, Vol. 24, No. 3, July 2008, pp. 295-312.
- [15] Ulrich, Xialing and Peters, David A., “Sinusoidal Locomotion of a Flexible Wing at High Reynolds Numbers,” *Journal of Fluids and Structures*, E-Version, December 2013, 10.1016/j.jfluidstructs.2013.11.017; Print Version: Vol. 45, February 7, 2014, pp. 15-27
- [16] Nowak, Morgan, Fei, Zhongyang, Peters, David A., and Prasad, J.V.R., “Improved Finite-State Inflow Convergence Through Use of a Blended Model,” Proceedings of the Fifth Decennial AHS Aeromechanics Specialists’ Conference, San Francisco, California, January 22-24, 2014.
- [17] Huang, Jianzhe, Nowak, Morgan, Peters, David, Prasad, J.V.R., “Converged Velocity Field for Rotor by a Blended Potential Flow Method,” Proceedings of the 70th Annual Forum of the American Helicopter Society, Montreal, Canada, May 20-22, 2014.



Jianzhe Huang, graduate research assistant
Department of Mechanical Engineering & Materials
Science
Washington University in St. Louis



David A. Peters, McDonnell Douglas Professor of
Engineering
Department of Mechanical Engineering & Materials
Science
Washington University in St. Louis



J.V. R. Prasad, Professor of Aerospace Engineering
School of Aerospace Engineering
Georgia Institute of Technology, Atlanta, Georgia